Surfaces and Interfaces 17 (2019) 100345

Contents lists available at ScienceDirect

Surfaces and Interfaces

journal homepage: www.elsevier.com/locate/surfin

Investigation of electrochemical performance of the biosynthesized α-Fe_2O_3 nanorods

A.K.H. Bashir[*,a,b], N. Mayedwa[a], K. Kaviyarasu[a,b], L.C. Razanamahandry[a,b], N. Matinise[a,b], K. Bharuth-Ram[c], M.B. Tchoula Tchokonté[d], F.I. Ezema[a,b,e], M. Maaza[a,b]

[a] UNESCO-UNISA Africa Chair in Nanosciences-Nanotechnology, Pretoria, PO Box 392, South Africa
[b] Nanosciences African Network (NANOAFNET), iThemba LABS-National Research Foundation, Somerset West, Western Cape Province, PO Box 722, South Africa
[c] Physics Department, Durban University of Technology, Durban, PO Box 1334, South Africa
[d] Department of Physics, University of the Western Cape, Private Bag X 17, Bellville 7535, South Africa
[e] Department of Physics and Astronomy, University of Nigeria, Nsukka, Nigeria

ARTICLE INFO

Keywords:
Biosynthesis
Haematite nanorods
Cyclic voltammetry and electrochemical

ABSTRACT

This study concerns with the development of a facile method for the biosynthesis of α-Fe_2O_3 nanorods through green method with an extract from *Persea Americana* seeds and the potential use of these nanords in the electrochemical applications. The α-Fe_2O_3 biosynthesized with an extract from *Persea Americana* seeds thereby was studied by the means of X-ray diffraction (XRD), Transmission Electron Microscopy (TEM), Energy Dispersive X-ray Spectroscopy (EDS), Ultraviolet–Visible (UV–vis) analysis, Fourier Transform Infra-Red (FT-IR) spectroscopy, Mössbauer spectroscopy and Cyclic voltammetry. X-ray diffraction (XRD) pattern of the sample determined the crystal structure of α-Fe_2O_3 nanorods. Transmission Electron Microscopy (TEM) measurements showed a nanorod-based morphology with average diameter of 50 nm and length of 400 nm. FTIR spectrospy spectrum confirmed the phase purity and chemical bond for the sample. The energy band gap E_g value obtained for α-Fe_2O_3 nanorods based on UV vis spectrum was 2.7 eV. Mössbauer results confirmed the weak ferromagnetic behaviour of the sample as well as the oxidization state. Cyclic voltammetry measurements of α-Fe_2O_3 nanorods sample coated on glassy carbon electrode (GCE) showed two oxidation peaks at 0.62 V and 0.88 V associated with reversible multi step oxidation of Fe to FeO and then Fe_2O_3. Electrochemical impedance spectroscopy studies revealed minimum charge transfer resistance R_{ct} value, suggesting that α-Fe_2O_3 nanorods prepared has good conductivity and can be used in electrochemical energy storage application.

1. Introduction

Haematite, α-Fe_2O_3 nanoparticles, is a type of iron oxides which, in fact, belongs to a broad group of magnetic nanomaterials. These classes of nanomaterials have received a considerable attention due to their wide applications in various fields such as magnetic sensors [1], catalysis [2], biomedicine [3], magnetic resonance imaging [4], data storage [5] and environmental remediation [6]. In particular, α-Fe_2O_3 nanoparticles have received increased interest because of their extraordinary magnetic properties compared to their bulk states. Moreover, their low cost, stability and non-toxicity, coupled with their diversity of applications, for instance, they can be used in pigments [7,8], lithium ion batteries and gas sensors [9,10], catalysis [11,12], optical and biomedical devices [12–14] water purification [15], solar energy conversion and magnetic materials [16], have made them as a promising material for investigation amongst all iron oxides.

Thermodynamically, haematite (α-Fe_2O_3) is the most stable form of iron oxide under ambient pressure. It crystallizes in the rhombohedral type structure with space group $R\bar{3}c$, $Z = 6$ [17]. Furthermore, it is an n-type semiconductor with band gap of 2.1 eV. On the other hand, the magnetic structure of the haematite (α-Fe_2O_3) is very complex, which varies from antiferromagnetic transition at Néel temperature ($T_N \approx 966$ K) to weak ferromagnetic (WFM) structure [18,19] at room temperature.

In general, the properties of haematite (α-Fe_2O_3) might be significantly changed by the synthesis conditions such as type of the precursor, annealing temperature, synthesis method and etc. Therefore, controlling the particle size and shape is extremely significant in the preparation haematite nanoparticles, since their physical and chemical properties depend greatly on the shape and particle size. However,

* Corresponding author.
E-mail address: abashiruwc@gmail.com (A.K.H. Bashir).

https://doi.org/10.1016/j.surfin.2019.100345
Received 8 April 2019; Received in revised form 9 June 2019; Accepted 19 June 2019
Available online 19 June 2019
2468-0230/ © 2019 Published by Elsevier B.V.

haematite (α-Fe_2O_3) nanoparticles of different shapes and sizes can be synthesised using various methods such as sol-gel method [20], hydrothermal technique [21], co-precipitation [22] and green chemistry [23,24]. The latter one has been used recently, and attracted much attention due to its multi advantages such as the easy preparation, low cost, non-toxicity and eco-friendly. In view of these advantages of the green chemistry method, many researches have been devoted to develop it as well as to understand the mechanism of formation of nanoparticles using this method [25,26].

The practical application of α-Fe_2O_3 as anode material has been widely investigated because of its high theoretical capacity. But, there are still some challenges facing α-Fe_2O_3 as a highly performance anode materials such as low electronic conductivity and large volume expansion during charge-discharge process which effects on fast capacity fading and poor rate capability. Several techniques are implemented to enhance the electrical conductivity of α-Fe_2O_3 by adding support conductive materials such as carbon [27], graphene [28], polyaniline [29] and polypyrrole [30]. However, there are still problems with cycling stability especially in high current densities. To improve the performances of α-Fe_2O_3 as anode especially in point of stable discharge cycling stability, another technique is used by synthesizing various nanostructure of α-Fe_2O_3, such as nanorod [31], nanotube [32] and nanosphere [33].

This research work combines between the advantages principles of the green chemistry method to synthesis nanoparticles and the practical application of the nanoparticles. Therefore, α-Fe_2O_3 nanorods have been successfully synthesized using *Persea Americana* seed extract and their electrochemical properties have been reported. *Persea Americana* seed contains various phytochemical [34] such as ascorbic and phenolic acids and avonoids which have been reported elsewhere [25] as effective reducing and capping agents for nanoparticles. The characterization of the sample synthesized and electrochemical properties are presented and discussed systematically.

2. Experimental

2.1. Persea americana seeds extract preparation

Fresh *Persea americanas* were purchased from Somerset Mall, Cape Town, South Africa. 80 g of seeds were obtained and cleaned thoroughly using deionized water and then heated at 60°C with 500 ml of deionized water in a glassy beaker for 24 h. The extract with dark brown colour was obtained and let to cool to ambient temperature. Then the extract was filtered several times using filter paper (Whatman no.1) to assure the purity of the extract from any residual impurity before using for the sample preparation.

2.2. α-Fe_2O_3 nanoparticles synthesis

The chemical salt, ($FeCl_3.9H_2O$, Sigma Aldrich 98%), used in this work was of analytical grade and used as received without any purification. The Fe_2O_3 sample was prepared by mixing 8 g of the iron metal salt ($FeCl_3.9H_2O$) with 100 ml of the extract and kept under constant stirring using a magnetic stirrer at 80°C for 6 h. The reddish brown precipitants that obtained were centrifuged at 4000 rpm and then cleaned with deionized water for many times before drying at 80°C for 12 h. Thereafter, the product was calcined at 500°C for 4 h using an open air furnace. Fig. 1 shows a flowchart to elucidate the biosynthesis of α-Fe_2O_3 nanorods using an extract from *Persea Americana* seeds. To explain the mechanism of formation of α-Fe_2O_3 nanorods, the phytochemicals of the *Persea Americana* seed such as ascorbic and phenolic acids and avonoids can serve both as effective reducing and capping agents for nanoparticles [24]. Therefore, the mechanism of formation of α-Fe_2O_3 nanorods was performed via three chemical reactions of the solvated Fe^{3+} ions with these phytochemicals of the *Persea Americana* see

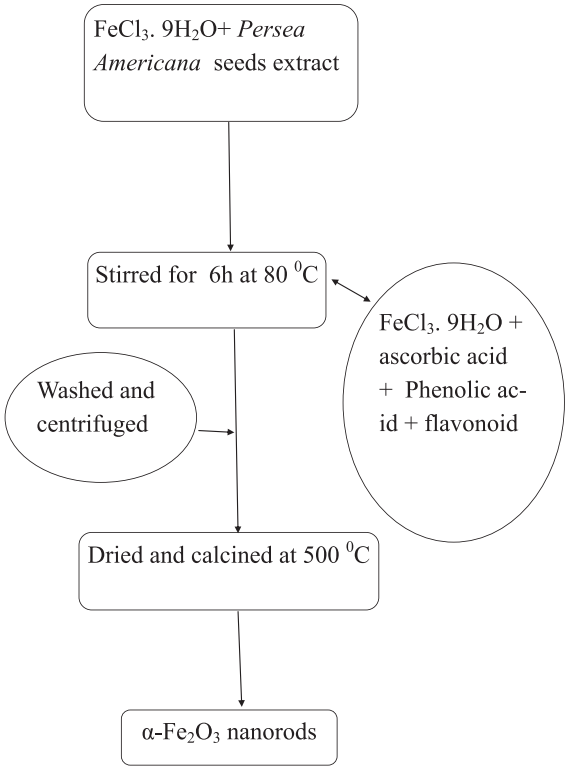

Fig. 1. Flowchart for the synthesis of α-Fe_2O_3 nanorods using an extract from *Persea Americana* seeds.

2.3. Characterization studies

In this work, various experimental techniques have been implemented in order to figure out the structural, morphological, elemental compositions, optical properties, magnetic behaviour and electrochemical analysis of α-Fe_2O_3 NPs. The crystalline structure of the sample was checked using A D8 advanced X-ray diffractometer over a scanning range of $2\theta = 10^{\circ}$–70°. TEM micrographs, SAED pattern and elemental compositions were obtained using a High Resolution Transmission Electron Microscope (HRTEM) (Philips Technai TEM) operated at 200 kV. The optical properties of the sample was determined using a Nicolette Evolution 100 Spectrometer (Thermo Electron Cooperation, UK) at room temperature over the range of 200–1000 nm. Fourier transform infrared (FT-IR) absorption spectrometer (Shimadzu 8400s spectrophotometer) was utilized to identify the chemical bondings over the measured range of 300–4000 cm^{-1}. Mössbauer spectroscopy investigation on the sample was obtained by recording the spectrum from ^{57}Fe nuclei at room temperature using the spectrometer MS-1104Em equipped with a $^{57}Co(Rh)$ source of gamma-radiation, where the Isomer shift was measured relative to the reference α-Fe_2O_3 at room temperature.

2.4. Electrochemical characterization

The electrochemical performances were tested on Autolab Potentiostat (CH Instruments, USA) electrochemical workstation with a three-electrode system, Glassy carbon electrode (GCE) as a working electrode with 0.071 cm^2 diameter, AgCl/Cl as a reference electrode and Pt wire as a counter electrode. Cyclic voltammetry (CV) and electrochemical impedance spectroscopy (EIS) techniques were used to understand the electrochemical properties of the α-Fe_2O_3 nanorods. In electrochemical experiments, 10 ml of 0.5 M KOH aqueous solution was used as the electrolyte over a potential range of −200 mV to +1000 mV. EIS measurements of α-Fe_2O_3 nanorods were measured in

0.5 M KOH solution and plotted in the form of complex plan diagram (Nyquist and bode plots) at a perturbation amplitude of 10 mV within a frequency range of 100 kHz to 100 mHz. All experimental solutions were de-oxygenated by bubbling with high purity argon gas for 15 min and blanketed with argon during all measurement.

2.4.1. Preparation of modified glassy carbon electrode

The small gram of the biosynthesized α-Fe_2O_3 nanorods was dissolved in ethanol and added 2 μl of 5% Nafion solution. The solution was ultra-sonicated using a warm water bath for 15 minutes to make a slurry solution. Alumina micro-polish (1.0, 0.3 and 0.05 mm alumina slurries) and polishing pads (Buehler, IL, USA) were used for polishing the surface area of a glassy carbon electrode before and after measurements. About 6 μl solution was drop-coated on the surface area of a glassy carbon electrode and allowed to dry at room temperature. The modified glassy carbon electrode (GCE/α-Fe_2O_3) was rinsed with deionized water to remove any excess adsorbed nanorods and was further used for electrochemical characterization. The modified GCE directly acted as the working electrode for electrochemical analysis.

3. Results and discussion

3.1. XRD

The structure and phase composition as well as particles size of α-Fe_2O_3 were identified using x-ray diffractometer (XRD). Fig. 2 showed that the sample synthesized has typically the characteristic XRD pattern of haematite α-Fe_2O_3 (ICDD card no. 33-0664) [35,36]. Moreover, the diffraction peaks can be indexed according to rhombohedral (hexagonal) structure α-Fe_2O_3 with space group $R\bar{3}C$ and lattice parameters a = 5.0327 Å and b = 13.7521 Å [37]. Thus, the observed peak positioned at 2θ: 24.16°, 33.12°, 35.63°, 40.64°, 49.47°, 54.08°, 57.59°, 62.45° and 63.99° coincide with the (012), (104), (110), (113), (024), (116), (018), (214) and (300) crystalline structures corresponding to α-Fe_2O_3 nanoparticles. The peak intensities are generally high for the sample, which indicate good crystallization with high amounts of haematite lattice. No extra peaks have been found in the XRD pattern and thereby confirming the formation of a pure α-Fe_2O_3 sample.

The value of the crystallite size was calculated based on Scherer's formula

$$D = \frac{K\lambda}{\beta \cos\theta} \quad (1)$$

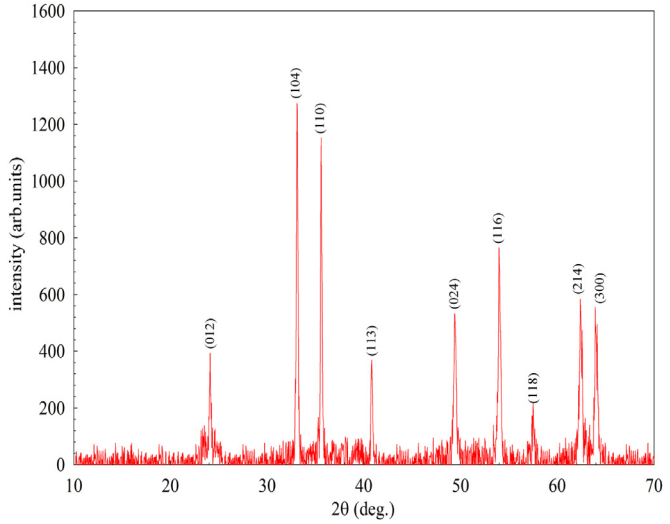

Fig. 2. XRD patterns for α-Fe_2O_3 nanorods synthesised using *Persea Americana* seeds extract.

where, D is the crystallite size in Å, $K \simeq 0.9$ is an empirical constant, λ = 1.5418 Å is the wavelength of the X-ray source, β is the effective full width at half maximum (FWHM) of the most intense peak and θ is diffraction angle at the most intense peak position. The crystallite sizes value yielded from XRD data based on Scherer's equation is approximately 45 nm for the sample. However, the estimation of Lattice parameters of the sample was obtained using Bragg's law:

$$n.\lambda = 2d.\sin\theta \quad (2)$$

where n is a positive integer represents the order of diffraction, λ is the wavelength of the incident beam, and d is the interplanar distance between planes of Miller indices h, k, and l. In the hexagonal symmetry, the relationship between interplanar distance, lattice parameters a and c, and h, k, and l can be expressed by the following equation

$$sin^2\theta = \frac{\lambda}{4}\left[\frac{4}{3}\left(\frac{h^2 + hk + k^2}{a^2}\right) + \left(\frac{1}{c}\right)^2\right] \quad (3)$$

Eq. (3) allows us to calculate the lattice parameters a and c for the sample synthesized. Thus, lattice parameter a, was calculated using the (110) plane with diffraction peak at 2θ = 35.5893 Å, while lattice parameter c was obtained using the (104) plane with diffraction peak at 2θ = 33.1195 Å. The lattice parameters of α-Fe_2O_3 sample was found to be a = 5.4095 Å and c = 13.1089 Å, which are consistent with the results of the previous reports [37].

3.2. FTIR studies

The FTIR technique is utilized to identify the functional groups (absorption bands) adsorbed on a surface of a material. These functional groups are greatly dependentdent on the crystalline structure and chemical composition of the material. The FTIR spectrum of α-Fe_2O_3 nanorods sample with highlights indicating the absorption range of each band is shown in Fig. 3. Two strong absorption bands were observed at 548 cm^{-1} and 452 cm^{-1} for the sample represent characteristic features of α-Fe_2O_3 and corresponds to metal oxygen stretching frequencies. The absorption band at 548 cm^{-1} refers to Fe-O deformation in the octahedral and tetrahedral sites while the other band at 452 cm^{-1} is attributed to FeO deformation in the octahedral site [40]. Noticeably, the intensity of the absorption band at 548 cm^{-1} is stronger than that at 452 cm^{-1}, which gives further evidence for the formation of α-Fe_2O_3 in

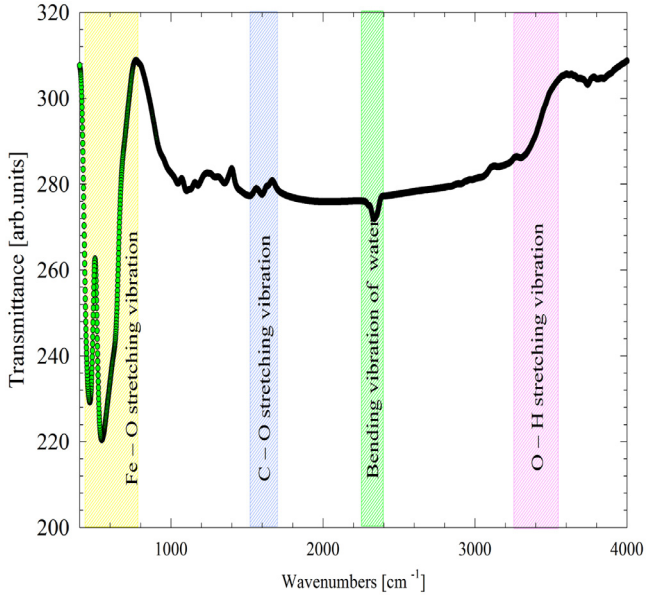

Fig. 3. FTIR spectrum of α-Fe_2O_3 nanorods with highlights indicating the positions of absorption peaks.

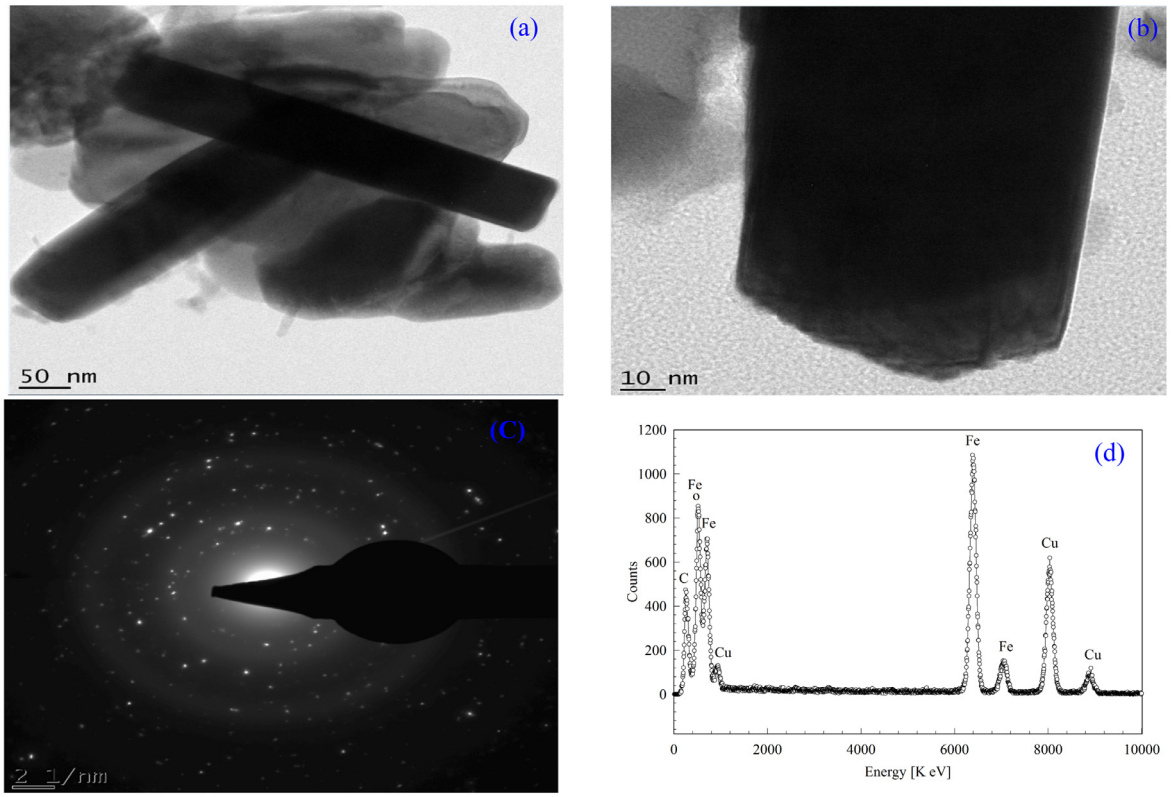

Fig. 4. Morphologies analysis of α-Fe_2O_3 nanorods: (a) and (b) TEM images of the sample at different magnifications (c) SAED pattern of the sample (d) EDS spectrum of the sample.

the nanords sample. The bands at 3350 and 1620 cm^{-1} are associated with the stretching vibration of water molecules [41]. Finally, the peak at 2340 cm^{-1} observed in the FTIR spectrum is assigned to the C—H stretch vibrations [42].

3.3. HTEM analysis

HTEM technique was used to confirm the shape and the particles size of α-Fe_2O_3 sample. The TEM imags, SAED patterns and EDS spectrum of the sample synthesised are depicted in Fig. 4. The TEM images of the sample at two different magnifications (see Fig. 4(a) and (b)) showed the nanorod-based morphology with average diameter and length of 50 nm and 400 nm, respectively. Such morphology of α-Fe_2O_3 nanoparticles has been observed and reported in some studies [38,39], particularly, when they prepared using ferric chloride as precursor, which in agreement with the results in the current report. The SAED patterns of the sample is illustrated in Fig. 4(c), which shows an increase in the diameter of ring patterns with small bright spots on the edge of each ring confirms the polynanocrystalline nature of the sample. Elemental constituents was checked with EDX spectrum as shown in Fig. 4(d), which indicates the sample is only formed by the elements Fe and O. The other elements that were observed in EDX spectrum such as C and Cu are referred to the carbon coated copper grid used for sample preparation, respectively.

3.4. Mössbauer spectroscopy study

The ^{57}Fe mössbauer spectrum recorded at room temperature (RT) for α-Fe_2O_3 nanorods sample is shown in Fig. 5 and shows sextet pattern confirming the appearance of magnetic behaviour in the sample. The spectrum was fitted based on the software RECOIL [43] and the ^{57}Fe mössbauer parameters of the sample were extracted. The value of hyperfine field B_{hf} obtained is 51.4(3) T which is associated with the

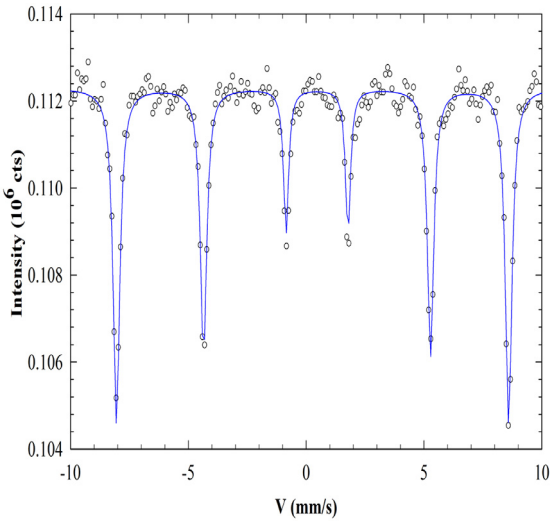

Fig. 5. ^{57}Fe Mössbauer spectrum recorded at room RT for α-Fe_2O_3 nanorods.

haematite phase α-Fe_2O_3 [44]. Furthermore, the values obtained for isomer shifts (*IS*) and quadruple shifts (ε_Q) are 0.37(1) mm/s and −0.11(1) mm/s, respectively, which also are consistent with the haematite phase α-Fe_2O_3 [44].The quadrupole interaction indicates Fe as Fe^{+3} because the *SI* value of 0.37 mm/s is similarly for Fe^{+3} ion [45]. Thus, we exclude the existence of Fe^{+2}, which possess a larger IS value which is approximately equal to 1.01 mm/s. At room temperature and ambient pressure, α-Fe_2O_3 experiences a weak ferromagnetic (WF) order [18,19] due to spins canting. Subsequently, the negative value of the quadrupole splitting obtained confirms the weak ferromagnetic behaviour [44] of the sample synthesised, which is a remarkable feature of haematite phase.

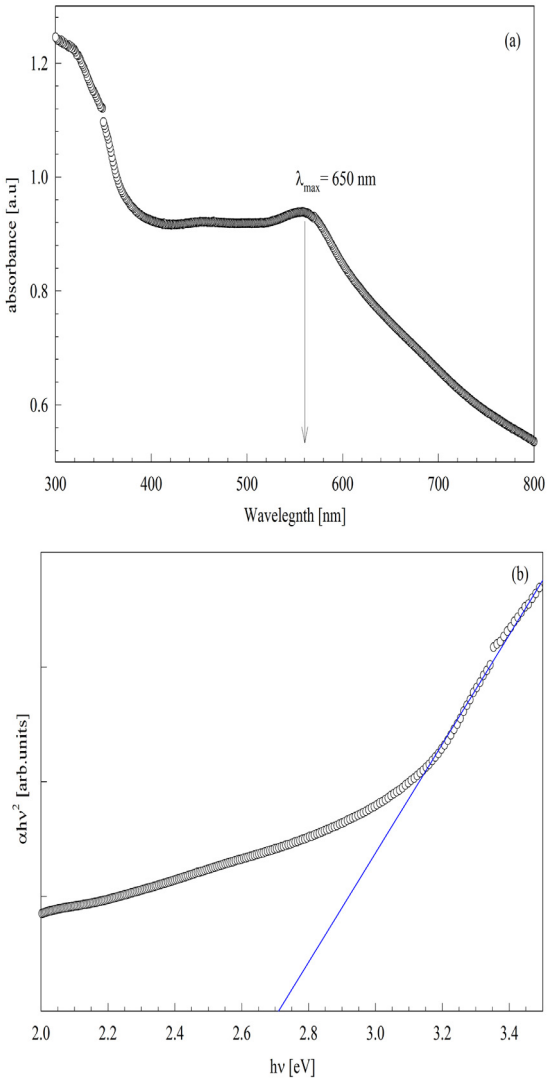

Fig. 6. UV Visible absorption spectrum of the α-Fe_2O_3 nanorods sample (a) UV VIS spectrum (b)band gap energy plot.

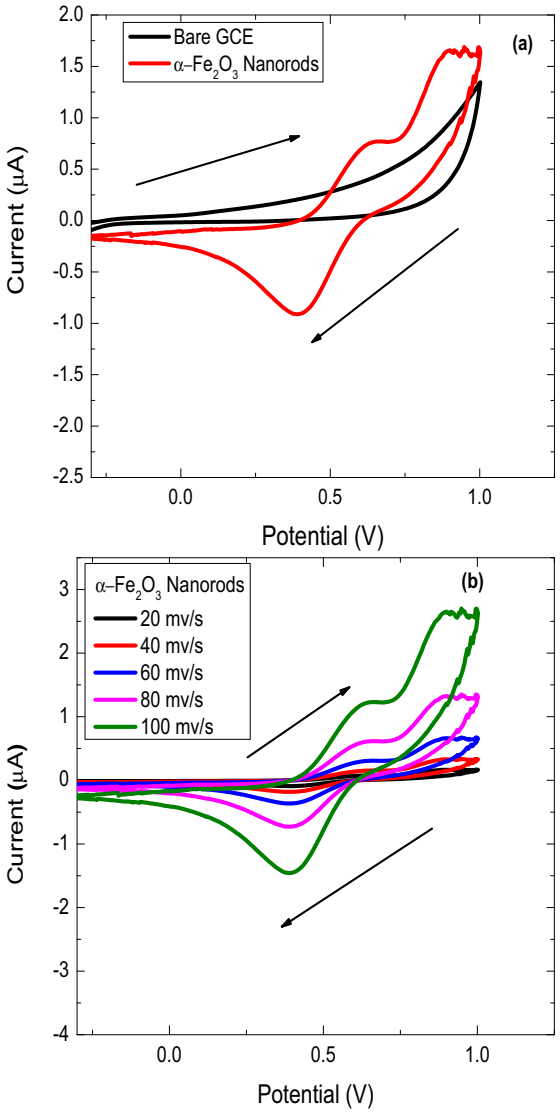

Fig. 7. Electrochemical performance of α-Fe_2O_3 nanorods coated on GCE in 0.5 M NaOH (a) CV curve of α-Fe_2O_3 nanorods on GCE in 0.5 M NaOH at a scan rate 50 $V.s^{-1}$ and (b) at different scan rates.

3.5. Optical properties

The optical absorption spectrum of the α-Fe_2O_3 nanorods sample in the wavelength range of 300–800 nm is shown in Fig. 6(a). The result shows that the absorption spectrum of the sample exhibits a strong absorption behaviour in the visible region wavelengths with a pronounced peak around 560 nm. This optical behaviour of α-Fe_2O_3 nanorods is ascribed to their intrinsic band gap absorption which result from the electron transitions between the valence and conduction bands [46]. Generally, the band gap of nanomaterials can be obtained using the following Tauc's equation:

$$(\alpha h\nu)^n = A(h\nu - E_g) \quad (4)$$

where h is Planck's constant, ν is the frequency of the incident photon, α is the absorption coefficient, A is a proportionality constant depends on the material, E_g is the band gap energy and n is a constant depends on the nature of the band gap energy [47]. The value assigned for the constant n might vary the between 2 or 1/2 depending on the nature of the band gap energy, which will take the value 2 for the direct band gap and 1/2 for the indirect band gap. However, E_g value can be extrapolated from the curve of $(\alpha h\nu)^n$ against $h\nu$, by extracting the value of the intercept from the energy axis ($h\nu$) when $(\alpha h\nu)^n = 0$. Thus, we have estimated the direct band gap for our sample by taking the value $n = 2$ for haematite [48]. Fig. 6(b) shows plot of $(\alpha h\nu)^n$ against $h\nu$ for α-Fe_2O_3 nanorods. The value of direct band gap E_g obtained for the sample is 2.7 eV.

3.6. Electrochemical behaviour

Electrochemical studies were reported in 0.5 M NaOH electrolyte for electrochemical characterization of α-Fe_2O_3 nanorods. Fig. 7(a) shows a typical Cyclic voltammetry results of α-Fe_2O_3 nanorods drop coated on glassy carbon electrode which can serve both as electrode as well as a bare glassy carbon electrode [49]. The measurement was performed in a potential ranges from −0.3 to 1.25 V at 50 $V.s^{-1}$ where two oxidation peaks are observed at 0.62 V and 0.88 V associated with reversible multi step oxidation of Fe to FeO and then Fe_2O_3 [50]. One reduction peak is observed at 0.39 V with good cycling stability after several cycles [51]. Fig. 7 (b) represents the CV curves of α-Fe_2O_3 nanorods sample modified on GCE with different sweep rates (20–100 $V.s^{-1}$) obtained in 0.5 M NaOH. It is observed that the anodic and cathodic peaks increased simultaneously with the increase in the scan rate [52].

Moreover, a pair of well-defined symmetric redox peaks ($I_{pa}/I_{pc} \approx$ 1.0) have been observed, even at high scan rates. The relationship

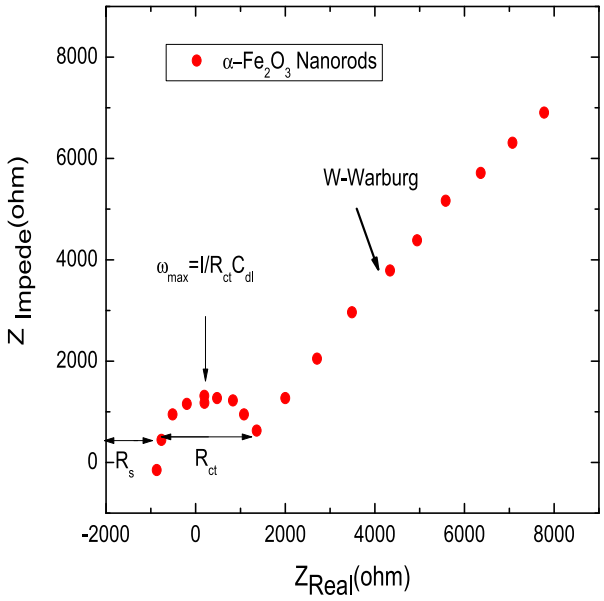

Fig. 8. Electrochemical impedance spectroscopy, Nyquist plot of α-Fe_2O_3 nanorods modified on modified on glassy carbon electrode (α-Fe_2O_3/GCE).

between the anodic peak current (I_{pa}) and the square root of scan rate for the scan rate range studied shows a good linear behaviour with a correlation coefficient of (R_2 = 0.9998), suggesting a diffused controlled redox reaction [53]. The kinetic studies further revealed that electro-oxidation of α-Fe_2O_3 nanorods sample is irreversible on GCE where it takes place through a two electrons ($2e^-$) and two protons ($2H^+$) process [54].

Electrochemical impedance spectroscopy (EIS) is employed to study the electrochemical behaviour of α-Fe_2O_3 nanorods as electrode. Fig. 8 shows the Nyquist impedance plot of the α-Fe_2O_3 nanorods electrode in a frequency ranges from 100 kHz to 0.01 Hz with an excitation signal of 5 mV at open circuit potential (0.44 V). The equivalent circuit was used for fitting the spectrum obtained from EIS data. The Nyquist plot (Fig. 8) shows two different regions, high frequency region with small loop of semicircle assigned to the charge transfer resistance (R_{ct}) and low frequency region representing with a straight line originated from Warburg impedance. This is indicating that the electrochemical performances are highly related to the interfacial charge-transfer process and diffusion control [55,56]. A minimum R_{ct} value suggests a smooth interfacial electron transfer process and thereby a higher specific pseudo-Faradaic capacitance while Warburg impedance is an indication of facile electrolyte diffusion to the surface of the electrodes [55,57]. These EIS data analysis findings reveal that α-Fe_2O_3 nanorods sample has good electronic conductivity as well as electrochemical stability which qualify them as a potential candidate for electrochemical energy storage application.

3.7. Conclusion

In this work, haematite α-Fe_2O_3 nanorods were synthesised with an extract from *Persea americanas* seeds which act as an effective reducing agent. The haematite phase of the sample synthesised was mainly confirmed from XRD pattern and Mössbauer technique which revealed that the oxidation state of the sample is Fe^{3+}. TEM analysis showed that the sample synthesized has nanorod-based structure while EDS spectrum confirmed the elemental constituents of the sample as Fe and O. UV vis spectrum of the sample showed a peak pronounced at 560 nm and the estimated energy gap was 2.7 eV. Electrochemical study on α-Fe_2O_3 nanorods synthesised with an extract from *Persea americanas* seeds proved that it is an electrochemically active with two oxidation and one reduction peaks at 0.88 V, 0.62 V and 0.39 V, respectively, associated with reversible multi step oxidation of Fe to Fe_2O_3. EIS study confirmed that α-Fe_2O_3 nanorods synthesised using *Persea americanas* has good conductivity and therefore is a potential candidate for electrochemical energy storage application.

Declaration of Competing Interest

All authors declare that there is no conflict of interest.

Acknowledgments

Support is acknowledged from the UNESCO-UNISA Africa Chair in Nanosciences for research funding (contract no. 90396898) and the Research Development Office of University of the Western Cape (UWC), South Africa.

References

[1] J. Kennedy, J. Leveneur, J. Turner, J. Futter, G.V.M. Williams, Applications of nanoparticle-based fluxgate magnetometers for positioning and location, Sens.Appl. Symp. (SAS), IEEE, 2014.
[2] K.K. Senapati, C. Borgohain, P. Phukan, Synthesis of highly stable $CoFe_2O_4$ nanoparticles and their use as magnetically separable catalyst for Knoevenagel reaction in aqueous medium, J. Mol. Catal. A Chem. 339 (2011) 24–31.
[3] A.K. Gupta, M. Gupta, Synthesis and surface engineering of iron oxide nanoparticles for biomedical applications, Biomaterials 26 (2005) 3995–4021.
[4] Z. Li, L. Wei, M. Gao, H. Lei, One-pot reaction to synthesize biocompatible magnetite nanoparticles, Adv. Mater. 17 (2005) 1001–1005.
[5] T. Hyeon, Chemical synthesis of magnetic nanoparticles, Chem. Commun. (2003) 927–934.
[6] M. Takafuji, S. Ide, H. Ihara, Z. Xu, Preparation of poly(1-vinylimidazole)-grafted magnetic nanoparticles and their application for removal of metal ions, Chem. Mater. 16 (2004) 1977–1983.
[7] D. Walter, Characterization of synthetic hydrous hematite pigments, Thermochim. Acta. 445 (2006) 195–199.
[8] S.R. Prim, M.V. Folgueras, M.A. De Lima, D. Hotza, Synthesis and characterization of hematite pigment obtained from a steel waste industry, J. Hazard. Mater. 192 (2011) 1307–1313.
[9] C. Wu, C. Wu, P. Yin, X. Zhu, C.O. Yang, Y. Xie, Synthesis of hematite (α-Fe_2O_3) nanorods: diameter-size and shape effects on their applications in magnetism, lithium ion battery, and gas sensors, J. Phys.Chem. B 110 (2006) 17806–17812.
[10] X. Gou, G. Wang, J. Park, H. Liu, J. Yang, Monodisperse hematite porous nanospheres: synthesis, characterization, and applications for gas sensors, Nanotechnology 19 (2008) 125606–125612.
[11] S.D. Tilley, M. Cornuz, K. Sivula, M. Grätzel, Light-induced water splitting with hematite: improved nanostructure and iridium oxidecatalysis, Angew. Chem. 122 (2010) 6549–6552.
[12] F. Herrera, A. Lopez, G. Mascolo, P. Albers, J. Kiwi, Catalytic combustion of orange II on hematite: surface species responsible for the dye degradation, Appl. Catal. B 29 (2001) 147–162.
[13] P. Tartaj, M.P. Morales, T. Gonzalez-Carreño, S. Veintemillas-Verdaguer, C.J. Serna, The iron oxides strike back: from biomedical applications to energy storage devices and photoelectrochemical water splitting, Adv. Mater. 23 (2011) 5243–5249.
[14] Y. Xu, G. Zhang, G. Du, Y. Sun, D. Gao, α-Fe_2O_3 nanostructures with different morphologies: additive-free synthesis, magnetic properties, and visible light photocatalytic properties, Mater. Lett. 92 (2013) 321–324.
[15] S. Zeng, K. Tang, T. Li, Z. Liang, D. Wang, Y. Wang, W. Zhou, Hematite hollow spindles and microspheres: selective synthesis,growth mechanisms, and application in lithium ion battery and water treatment, J. Phys. Chem. C. 111 (2007) 10217–10225.
[16] I. Thomann, B.A. Pinaud, Z. Chen, B.M. Clemens, T.F. Jaramillo, M.L. Brongersma, Plasmon enhanced solar-to-fuel energy conversion, Nano Lett. 11 (2011) 3440–3446.
[17] R. Cornell, U. Schwertmann, The Iron Oxides: Structure, Properties, Reactions, Occurences and Uses, Second ed., Wiley, Weinheim, 2003.
[18] A.H. Morrish, Canted Antiferromagnetism: Hematite, World Scientific, Singapore, 1994.
[19] P. Majewski, B. Thierry, Crit. Rev. Solid State Mater. Sci. 32 (3–4) (2007) 203–215.
[20] . S. Demirci, M. Yurddaskal, T. Dikici, . C. Saroğlu, Fabrication and characterization of novel iodine doped hollow and mesoporous hematite (Fe_2O_3) particles derived from sol-gel method and their photocatalytic performances, J. Hazard. Mater. 345 (2018) 27–37.
[21] M. Tadic, M. Panjan, V. Damnjanovic, I. Milosevic, Magnetic properties of hematite (α-Fe_2O_3) nanoparticles prepared by hydrothermal synthesis method, Appl. Surf. Sci. 320 (2014) 183–187.
[22] M. Farahmandjou, F. Soflaee, Synthesis and characterization of α-Fe_2O_3 nanoparticles by simple co-precipitation method, Phys. Chem. Res. 3 (2015) 191–196.
[23] A.T. Khalil, M. Ovais, I. Ullah, M. Ali, Z.K. Shinwari, M. Maaza, Biosynthesis of iron oxide (Fe_2O_3) nanoparticles via aqueous extracts of *Sageretia thea* (osbeck.) and

their pharmacognostic properties, Green Chem. Lett. Rev. 10 (2017) 186–201.
[24] A. K. H. Bashir, C. M. Furqan, K. Bharuth-Ram, K. Kaviyarasu, M. B. T. Tchokont, M. Maaza, Structural, optical and Mössbauer investigation on the biosynthesized α-Fe_2O_3: study on different precursors, Physica E 111 (2019) 152–157.
[25] N. Matinise, X.G. Fuku, K. Kaviyarasu, N. Mayedwa, M. Maaza, ZnO nanoparticles via *Moringa oleifera* green synthesis: physical properties & mechanism of formation, Appl. Surf. Sci. 406 (2017) 339–347.
[26] N. Mayedwa, N. Mongwaketsi, S. Khamlich, K. Kaviyarasua, N. Matinise, M. Maaza, Green synthesis of nickel oxide, palladium and palladium oxides synthesized via aspalathus linearis natural extracts: physical properties & mechanism of formation, Appl. Surf. Sci. 446 (2018) 266–272.
[27] R. Liu, C. Zhang, Q. Wang, C. Shen, Y. Wang, Y. Dong, N. Zhang, M. Wu, Facile synthesis of α-Fe_2O_3@c hollow spheres as ultra-long cycle performance anode materials for lithium ion battery, J. Alloys Compd. 742 (2018) 490.
[28] M. Wu, M. Wu, J. Chen, C. Wang, F. Wang, B. Yi, W. Su, Z. Wei, S. Liu, Self-assembly of Fe_2O_3 nanotubes on graphene as an anode material for lithium ion batteries, J. Alloys Compd. 750 (2018) 871.
[29] J. Guo, L. Chen, G. Wang, X. Zhang, F. Li, In situ synthesis of $SnO_2Fe_2O_3$@polyaniline and their conversion to $SnO_2Fe_2O_3$c composite as fully reversible anode material for lithium-ion batteries, J. Power Sources 246 (2014) 862.
[30] J. Liu, W. Zhou, L. Lai, H. Yang, S.H. Lim, Y. Zhen, T. Yu, Z. Shen, J. Lin, Three dimensionals α-Fe_2O_3/polypyrrole (ppy) nanoarray as anode for micro lithium ion batteries, Nano Energy 2 (2013) 726.
[31] Y.M. Lin, P.R. Abel, A. Heller, C.B. Mullins, α-Fe_2O_3 nanorods as anode material for lithium ion batteries, J. Phys. Chem. Lett. 2 (2011) 2885.
[32] J. Chen, L. Xu, W. Li, X. Gou, α-Fe_2O_3 nanotubes in gas sensor and lithium-ion battery applications, Adv. Mater. 17 (2005) 582.
[33] B. Wang, J.S. Chen, H.B. Wu, Z. Wang, X.W.D. Lou, Quasiemulsion-templated formation of α-Fe_2O_3 hollow spheres with enhanced lithium storage properties, J. Am. Chem. Soc. 133 (2011) 17146.
[34] Y. Ge, X. Si, J. Cao, Z. Zhou, W. Wang, W. Ma, Morphological characteristics, nutritional quality, and bioactive constituents in fruits of two avocado (*Persea americana*) varieties from hainan province, china, J. Agric. Sci. 9 (2) (2017).
[35] H. Liu, Y. Wei, Y. Sun, The formation of hematite from ferrihydrite using fe (II) as a catalyst, J. Mol. Catal. A Chem. 226 (2005) 135–1340.
[36] J. Hua, J. Gengsheng, Hydrothermal synthesis and characterization of monodisperse α-Fe_2O_3 nanoparticles, Mater. Lett. 63 (2009) 2725–2727.
[37] A.S. Teja, P.Y. Koh, Synthesis, properties, and applications of magnetic iron oxide nanoparticles, Prog. Cryst. Growth Charact. Mater. 55 (2009) 22–45.
[38] V.A.N. De Carvalho, R.A.D.S. Luz, B.H. Lima, F.N. Crespilho, E.R. Leite, F.L. Souza, Highly oriented hematite nanorods arrays for photoelectrochemical water splitting, J. Power Sources 205 (2012) 525–529.
[39] H.K. Mulmudi, N. Mathews, X.C. Dou, L.F. Xi, S.S. Pramana, Y.M. Lam, S.G. Mhaisalkar, Controlled growth of hematite (α-Fe_2O_3) nanorod array on fluorine doped tin oxide: Synthesis and photoelectrochemical properties, Electrochem. Commun. 13 (2011) 951–954.
[40] G. Wu, X. Tan, G. Li, C. Hu, Effect of preparation method on the physical and catalytic property of nanocrystalline α-Fe_2O_3, J. Alloys Compd. 504 (2010) 371–376.
[41] E. Darezereshki, One-step synthesis of hematite (α-Fe_2O_3) nano-particles by direct thermal-decomposition of maghemite, Mater Lett. 65 (2011) 642–645.
[42] F. Bakhtiari, E. Darezereshki, One-step synthesis of tenorite (CuO) nano-particles from Cu_4 (SO_4) $(OH)_6$ by direct thermal-decomposition method, Mater Lett 65 (2011) 171.
[43] K. Lagarec, D.G. Rancourt, Recoil: Mössbauer spectral analysis software for windows, 1998.
[44] M. Mohapatra, S. Layek, S. Anand, H.C. Verma, B.K. Mishra, Structural and magnetic properties of Mg-doped nano-α-Fe_2O_3 particles synthesized by surfactant mediated precipitation technique, Phys. Status Solidi B 250 (2012) 65–72.
[45] S. Lyubutin, N.E. Gervits, S.S. Starchikov, C.-R. Lin, Y.-T. Tseng, K.-Y. Shih, C.-C. Wang, I.-H. Chen, Y.L. Ogarkova, N.Y. Korotkov, Magnetic and Mössbauer spectroscopy studies of hollow microcapsules made of silica-coated $CoFe_2O_4$ nanoparticles, Smart Mater. Struct 25 (2016) 015022.
[46] J. Yu, X. Yu, Hydrothermal synthesis and photocatalytic activity of zinc oxide hollow spheres, Environ. Sci. Technol 42 (13) (2008) 4902–4907.
[47] R. Branek, H. Kisch, Tuning the optical and photoelectrochemical properties of surface-modified TiO_2, Photochem. Photobiol. Sci. 7 (2008) 40–48.
[48] J.I. Pankove, Optical Processes in Semiconductors, Prentice-Hall Inc., Englewood Cliff, New Jersey, 1971, pp. 34–86.
[49] N.L. Wu, S.Y. Wang, C.Y. Han, D.S. Wu, L.R. Shiue, Electrochemical capacitor of magnetite in aqueous electrolytes, J Power Sources 113 (2003) 173–178.
[50] S.Y. Wang, N.L. Wu, Operating characteristics of aqueous magnetite electrochemical capacitors, J. Appl. Electrochem. 33 (2003) 345–348.
[51] S.C. Pang, W.H. Khoh, S.F. Chin, Nanoparticulate magnetite thin films as electrode materials for the fabrication of electrochemical capacitors, J. Mater. Sci. 45 (2010) 5598–5604.
[52] S.Y. Wang, K.C. Ho, S.L. Kuo, N.L. Wu, Investigation on capacitance mechanisms of Fe_3O_4 electrochemical capacitors, J. Electrochem. Soc. 153 (2006) A75–A80.
[53] J. Chen, K. Huang, S. Liu, Hydrothermal preparation of octadecahedron Fe_3O_4 thin film for use in an electrochemical supercapacitor, Electrochim Acta 55 (2009) 1–5.
[54] H. Sun, B. Chen, X. Jiao, Z. Jiang, Z. Qin, D. Chen, Solvothermal synthesis of tunable electroactive magnetite nanorods by controlling the side reaction, J. Phys. Chem. C 116 (2012) 5476–5481.
[55] X. Fuku, K. Kaviyarasu, N. Matinise, M. Maaza, Punicalagin green functionalized $Cu/Cu_2O/ZnO/CuO$ nanocomposite for potential electrochemical transducer and catalyst nanoscale res, Lett. 11 (2016) 1–12.
[56] N. Matinise, K. Kaviyarasu, N. Mongwaketsi, S. Khamlich, L. Kotsedi, N. Mayedwa, M. Maaza, Green synthesis of novel zinc iron oxide ($ZnFe_2O_4$) nanocomposite via moringa oleifera natural extract for electrochemical applications, Appl. Surf. Sci. 446 (2018) 66–73.
[57] R. Ramya, R. Sivasubramanian, M.V. Sangaranarayanan, Conducting polymers-based electrochemical supercapacitors—progress and prospects, Electrochem. Acta 101 (2013) 109–129.